

## Article

# Enhancement of AFB<sub>1</sub> Removal Efficiency via Adsorption/Photocatalysis Synergy Using Surface-Modified Electrospun PCL-g-C<sub>3</sub>N<sub>4</sub>/CQDs Membranes

Liangtao Yao <sup>1</sup>, Changpo Sun <sup>2</sup>, Hui Lin <sup>1</sup>, Guisheng Li <sup>3</sup>, Zichao Lian <sup>3</sup>, Ruixin Song <sup>1</sup>, Songlin Zhuang <sup>1</sup> and Dawei Zhang <sup>1,4,\*</sup>

<sup>1</sup> Engineering Research Center of Optical Instrument and System, Ministry of Education and Shanghai Key Lab of Modern Optical System, University of Shanghai for Science and Technology, No.516 Jungong Road, Shanghai 200093, China; slzhuang@usst.edu.cn (S.Z.)

<sup>2</sup> Standards and Quality Center of National Food and Strategic Reserves Administration, No.25 Yuetan North Street, Xicheng District, Beijing 100834, China

<sup>3</sup> Department of Chemistry, College of Science, University of Shanghai for Science and Technology, No.516 Jungong Road, Shanghai 200093, China

<sup>4</sup> Fujian Provincial Key Laboratory for Advanced Micro-Nano Photonics Technology and Devices, Research Center for Photonics Technology, Quanzhou Normal University, Quanzhou 362000, China

\* Correspondence: dwzhang@usst.edu.cn

**Abstract:** Aflatoxin B<sub>1</sub> (AFB<sub>1</sub>) is a highly toxic mycotoxin produced by aspergillus species under specific conditions as secondary metabolites. In this study, types of PCL (Polycaprolactone) membranes anchored (or not) to g-C<sub>3</sub>N<sub>4</sub>/CQDs composites were prepared using electrospinning technology with (or without) the following surface modification treatment to remove AFB<sub>1</sub>. These membranes and g-C<sub>3</sub>N<sub>4</sub>/CQDs composites were characterized by SEM, TEM, UV-vis, XRD, XPS and FTIR to analyze their physical and chemical properties. Among them, the modified PCL-g-C<sub>3</sub>N<sub>4</sub>/CQDs electrospun membranes exhibited an excellent ability to degrade AFB<sub>1</sub> via synergistic effects of adsorption and photocatalysis, and the degradation rate of 0.5 µg/mL AFB<sub>1</sub> solution was observed to be up to 96.88% in 30 min under visible light irradiation. Moreover, the modified PCL-g-C<sub>3</sub>N<sub>4</sub>/CQDs electrospun membranes could be removed directly after the reaction process without centrifugal or magnetic separation, and the regeneration was a green approach synchronized with the reaction under visible light avoiding physical or chemical treatment. The mechanism of adsorption by electrostatic attraction and hydrogen bonding interaction was revealed and the mechanism of photodegradation of AFB<sub>1</sub> was also proposed based on active species trapping experiments. This study illuminated the highly synergic adsorption and photocatalytic AFB<sub>1</sub> removal efficiency without side effects from the modified PCL-g-C<sub>3</sub>N<sub>4</sub>/CQDs electrospun membranes, thereby offering a continual and green solution to AFB<sub>1</sub> removal in practical application.

**Keywords:** PCL electrospun membranes; aflatoxin B<sub>1</sub>; adsorption; photocatalysis; g-C<sub>3</sub>N<sub>4</sub>/CQDs; visible light



**Citation:** Yao, L.; Sun, C.; Lin, H.; Li, G.; Lian, Z.; Song, R.; Zhuang, S.; Zhang, D. Enhancement of AFB<sub>1</sub> Removal Efficiency via Adsorption/Photocatalysis Synergy Using Surface-Modified Electrospun PCL-g-C<sub>3</sub>N<sub>4</sub>/CQDs Membranes. *Biomolecules* **2023**, *13*, 550. <https://doi.org/10.3390/biom13030550>

Academic Editors: Deng-Guang Yu, Wenliang Song and Bahman Anvari

Received: 14 January 2023

Revised: 18 February 2023

Accepted: 7 March 2023

Published: 17 March 2023



**Copyright:** © 2023 by the authors. Licensee MDPI, Basel, Switzerland. This article is an open access article distributed under the terms and conditions of the Creative Commons Attribution (CC BY) license (<https://creativecommons.org/licenses/by/4.0/>).

## 1. Introduction

At present, the biological contamination of food has been paid more and more attention, along with the issue of food safety. Mycotoxin contamination is one of the main factors causing food safety problems. There are many kinds of mycotoxins, among which aflatoxin B<sub>1</sub> (AFB<sub>1</sub>) is the most toxic biological toxin food produced by aspergillus species so far. Its toxicity is 10 times that of potassium cyanide and 68 times that of arsenic, and it is classified as a class I human carcinogen by the International Agency for Research on Cancer (IARC) [1]. AFB<sub>1</sub> can easily enter the human food chain and threaten people's health. In order to ensure human health from the harm of AFB<sub>1</sub>, international organizations and countries around the world have determined the maximum tolerable limits of AFB<sub>1</sub> in

various foods. In the European Commission [2], the maximum limits are 2 µg/kg for AFB<sub>1</sub> in edible oils, cereals and cereal products. In China [3], the maximum limits of AFB<sub>1</sub> are set at 20 µg/kg for peanut and maize oils, and 10 µg/kg for the other vegetable oils. In the United States [4], the maximum limits of total aflatoxins (AFB<sub>1</sub> + AFB<sub>2</sub> + AFG<sub>1</sub> + AFG<sub>2</sub>) in all foods (except milk) are 20 µg/kg; acceptable levels of AFM<sub>1</sub> in milk and dairy products are 0.5 µg/kg.

Studies have shown that intake of large amounts of AFB<sub>1</sub> in a short time can lead to liver damage, such as liver tissue hemorrhage and acute hepatitis. To reduce or eliminate the adverse effects caused by AFB<sub>1</sub>, on the one hand, it is necessary to control the growth of the aspergillus species or hold back the arise of AFB<sub>1</sub> [5]; on the other hand, the symptoms of AFB<sub>1</sub> poisoning can be effectively relieved by taking animal function regulators (curcumin) or antiaflatoxin bacteria (probiotics) [6]. Furthermore, we need to develop various effective and practical methods for the detoxification of AFB<sub>1</sub> [7]. Adsorption is a widely used method to decrease aflatoxin contamination. There has been a series of studies on the elimination of AFB<sub>1</sub> with adsorbents. Ma et al. applied copper-based metal-organic frameworks (MOFs) to synthesize the porous carbonaceous materials as sorbents for the removing of AFB<sub>1</sub> from plant oils, and removed more than 90% of AFB<sub>1</sub> within 30 min [8]. Phillips et al. synthesized a highly active sodium bentonite clay with enhanced AFB<sub>1</sub> sorption efficacy compared with bentonite clay and other clays [9]. Karmanov et al. studied the performance of adsorption-desorption of aflatoxin B<sub>2</sub> (AFB<sub>2</sub>) using lignins obtained from several cultivated and medicinal plants in an in vitro simulated gastrointestinal tract environment; lignins from ledum and jerusalem artichoke exhibited the highest AFB<sub>2</sub> adsorption capacity, and the chemisorption mechanisms played the most leading role [10]. However, the adsorption capacity gradually decreases as the adsorbents are saturated with the adsorbed AFs. In addition, some adsorbents are short of reusability due to the shortage of environmentally friendly regeneration methods. For instance, common powder adsorbents usually need centrifuge separation for adsorbents recovery [11], and the regeneration process usually requires solvent washing under acidic/alkaline conditions or undergoing calcination treatment, which would inevitably release pernicious chemicals into the environment [12].

As we all know, adsorption membranes prepared by electrospinning technology have attracted sense of attention in wastewater treatment due to their large specific surface area [13,14]. Many kinds of pristine electrospinning polymer adsorption membranes or electrospinning polymer adsorption membranes containing additives (such as graphene oxide [15], silica [16], and carbon nanotubes [17]) were developed to adsorb organic pollutants or heavy metal ions [18,19]. These membranes were easy to separate from the reaction substrate after adsorption reaction, thus avoiding centrifugal separation and possible secondary pollution. Therefore, it is a reasonable strategy to use electrospun membranes to absorb AFB<sub>1</sub> in an aqueous medium. However, these electrospun membranes still need to be treated by chemical or physical methods for regeneration. Are there recyclable membranes that can not only degrade AFB<sub>1</sub> efficiently, but also avoid releasing harmful chemicals to the environment during regeneration?

Photocatalytic technology is a newly developed technology to degrade pollutants under mild or gentle conditions including AFB<sub>1</sub> [20,21]. In the photocatalytic process, When the light with appropriate energy irradiates the photocatalysts, the electrons (e<sup>−</sup>) are excited from the valence band to the conduction band leaving behind holes (h<sup>+</sup>) [22]. Then, these photogenerated charges (e<sup>−</sup> and h<sup>+</sup>) migrate from the inner of the photocatalysts to the surface of the photocatalysts. These photogenerated charges interact with H<sub>2</sub>O, O<sub>2</sub> or OH<sup>−</sup> around to produce •OH and •O<sub>2</sub><sup>−</sup>, which can attack the pollutant molecules into smaller fragments, even CO<sub>2</sub> or H<sub>2</sub>O [23]. Compared with traditional treatment methods, photocatalysis technology is environmentally friendly and low-cost. Inspired by the process mentioned above, it is an attractive strategy to develop a kind of green and recyclable membrane that combines adsorption and photocatalysis techniques to

degrade AFB<sub>1</sub> synergistically through electrospinning technology, overcoming difficulties in separating traditional adsorbents and photocatalysts.

Among the wide variety of polymers that can be used for electrospinning [24,25], polycaprolactone (PCL) has attracted extensive interest due to its availability, non-toxicity, and stability [26,27]. More importantly, the electrospun membranes prepared by PCL have excellent mechanical properties [28]. In this paper, PCL was chosen as the raw material of electrospun membranes. In order to overcome the disadvantage of poor adsorption capacity of the PCL electrospun membranes, surface modification technology was used to functionalize the membranes. Polydopamine (PDA) modification inspired by the excellent adhesion of *Mytilus edulis* foot has been widely used in membrane surface modification. Dopamine (DA) can self-polymerize to form a PDA layer coating at plenty of substrates under alkaline conditions or air atmosphere [29], which can improve the hydrophilicity and mechanical properties of the modified membranes. Furthermore, the phenolic hydroxyl groups on the surface of the PDA layer can be used to conjugate with amino-containing compounds to capture target molecules intentionally. So far, it has been reported that polyethyleneimine (PEI) [30], polyacrylamide (PAAM) [31], and other amino-containing compounds were grafted onto PDA-modified membranes to adsorb CO<sub>2</sub>, dye molecules, protease and other substances. In this study, we used PEI conjugate onto PDA-modified PCL electrospun membranes to adsorb AFB<sub>1</sub>.

In terms of photocatalysts, graphitic carbon nitride (g-C<sub>3</sub>N<sub>4</sub>), a metal-free semiconductor, has attracted wide attention due to its environmental friendliness, easy modification, and proper band gap [32]. However, the high recombination rate of photogenerated charges and poor spectral response range have become crucial issues for pristine g-C<sub>3</sub>N<sub>4</sub> [33]. Metal/non-metal element doping [34,35], construction of heterojunction [36], and other strategies were used to optimize the photocatalytic performance of g-C<sub>3</sub>N<sub>4</sub>. Carbon quantum dots (CQDs), a “zero-dimensional” nanomaterial, has become one of the most promising co-catalysts due to their excellent electron transfer ability and up-converting photoluminescence [37]. Therefore, it is a reasonable way to modify g-C<sub>3</sub>N<sub>4</sub> with CQDs to enhance visible light absorption as well as reduce the recombination of photogenerated charges [38]. The raw materials (such as urea, melamine, citric acid, sucrose, etc.) required for the preparation of CQDs and g-C<sub>3</sub>N<sub>4</sub> are easy to obtain and the preparation process is simple, which is favorable for practical applications. In this paper, g-C<sub>3</sub>N<sub>4</sub>/CQDs composites were used for the photocatalytic degradation of AFB<sub>1</sub> under visible light.

Herein, the flexible PCL-g-C<sub>3</sub>N<sub>4</sub>/CQDs electrospun membranes were successfully prepared using electrospinning technology. The surface of electrospun membranes were modified by PDA and PEI to remove AFB<sub>1</sub> continuously. To study the synergistic effect of adsorption and photocatalysis, comparative experiments were carried out using pristine PCL electrospun membranes, modified PCL electrospun membranes, PCL-g-C<sub>3</sub>N<sub>4</sub>/CQDs electrospun membranes and modified PCL-g-C<sub>3</sub>N<sub>4</sub>/CQDs electrospun membranes. The adsorption mechanism and the photocatalytic degradation mechanism of AFB<sub>1</sub> were investigated in the presence of different sacrificial agents. Moreover, the effect of recycling on the adsorption and photocatalytic efficiency was also evaluated. The work presented in this paper has potential practical value for the degradation of AFB<sub>1</sub>, which has plagued the food industry for a long time.

## 2. Experiment

### 2.1. Materials and Reagents

AFB<sub>1</sub> was purchased from Beijing Puhuashi Technology Development Co., Ltd. (Beijing, China). and dissolved to a certain concentration with deionized water. Urea (≥99.0% purity), anhydrous citric acid (≥99.0% purity), anhydrous methanol (≥99.0% purity) polycaprolactone (PCL,  $M_w \approx 80,000$ ), dopamine hydrochloride (AR, 99.5%), polyethyleneimine (PEI,  $M_w \approx 10,000$ ), N,N-dimethylformamide (DMF, AR, 99.5%), hexafluoroisopropanol (HFIP, AR, 99.5%), sodium hydroxide (AR, 99.5%) and Tris-HCl buffer (pH = 8.5) were purchased from Jingji Co., Ltd. (Suzhou, China). Glacial acetic acid (for HPLC, ≥99.9%),

methanol (for HPLC,  $\geq 99.9\%$ ), trifluoroacetate (for HPLC,  $\geq 99.5\%$ ) and acetonitrile (for HPLC,  $\geq 99.9\%$ ) were purchased from Macklin Biochemical Co., Ltd. (Shanghai, China). All reagents were used without any further purification. Dialysis bags were purchased from Shanghai yuan ye Bio-Technology Co., Ltd. (Shanghai, China). The deionized water used in this work was purified using the Millipore system purchased from Merck Co., Ltd. (Shanghai, China).

## 2.2. Preparation of $g\text{-C}_3\text{N}_4/\text{CQDs}$ Composites

Powdered  $g\text{-C}_3\text{N}_4$  was prepared by calcining urea at  $550\text{ }^\circ\text{C}$  for 3 h ( $5\text{ }^\circ\text{C}/\text{min}$ ). CQDs were synthesized through a facile hydrothermal method according to the improved method in reference [39]. Briefly, a certain amount of urea and citric acid with a mass ratio of 48:19 were fully dissolved in DMF. Then the solution was transferred to a polytetrafluoroethylene reactor, followed by placing it in a drying furnace at  $180\text{ }^\circ\text{C}$  for 6 h. After the reaction, on cooling to room temperature, the obtained red solution was centrifuged at a speed of  $8000\text{ r}\cdot\text{min}^{-1}$  for 10 min to remove the large deposit, and dialysis was carried out in a dialysis bag with a molecular weight of 500 Da for 48 h. Finally, the CQDs were obtained after freeze-drying treatment.

In a typical preparation of  $g\text{-C}_3\text{N}_4/\text{CQDs}$  composites, a certain amount of  $g\text{-C}_3\text{N}_4$  was dissolved in anhydrous methanol. Then, CQDs were added into the above solution, stirred and ultrasonicated for 1 h, respectively. After the suspension was dried at  $60\text{ }^\circ\text{C}$  for 6 h,  $g\text{-C}_3\text{N}_4/\text{CQDs}$  composites were obtained. The photocatalytic degradation performance of  $g\text{-C}_3\text{N}_4/\text{CQDs}$  samples with different contents of CQDs (0.1%, 0.3%, 0.5%, and 0.7%) and pristine  $g\text{-C}_3\text{N}_4$  can be seen in Figure S1, we determined that the mass ratio of CQDs in  $g\text{-C}_3\text{N}_4/\text{CQDs}$  composites was 0.5% in this study.

## 2.3. Preparation of Modified PCL- $g\text{-C}_3\text{N}_4/\text{CQDs}$ Electrospun Membranes

The modified PCL- $g\text{-C}_3\text{N}_4/\text{CQDs}$  electrospun membranes were prepared by electrospinning and the following surface modification treatment. The schematic illustration was shown in Figure 1. Typically, 0.2 g  $g\text{-C}_3\text{N}_4/\text{CQDs}$  composites were added into 10 mL HFIP and ultrasonicated for 1 h to fully disperse. Subsequently, 1 g PCL was added and stirred for 12 h at  $50\text{ }^\circ\text{C}$  to obtain a yellow-grey solution. Then loaded the prepared solution into a 10 mL plastic syringe with a metal needle. The syringe was driven by a hydraulic pump for electrospinning at a flow rate of  $2.5\text{ mL}/\text{h}$ . The applied voltage during electrospinning was 20 kV and the distance from the aluminum foil surface to the metallic needle was 15 cm. After electrospinning, the PCL- $g\text{-C}_3\text{N}_4/\text{CQDs}$  electrospun membranes were dried at  $45\text{ }^\circ\text{C}$  in a drying furnace for 12 h.

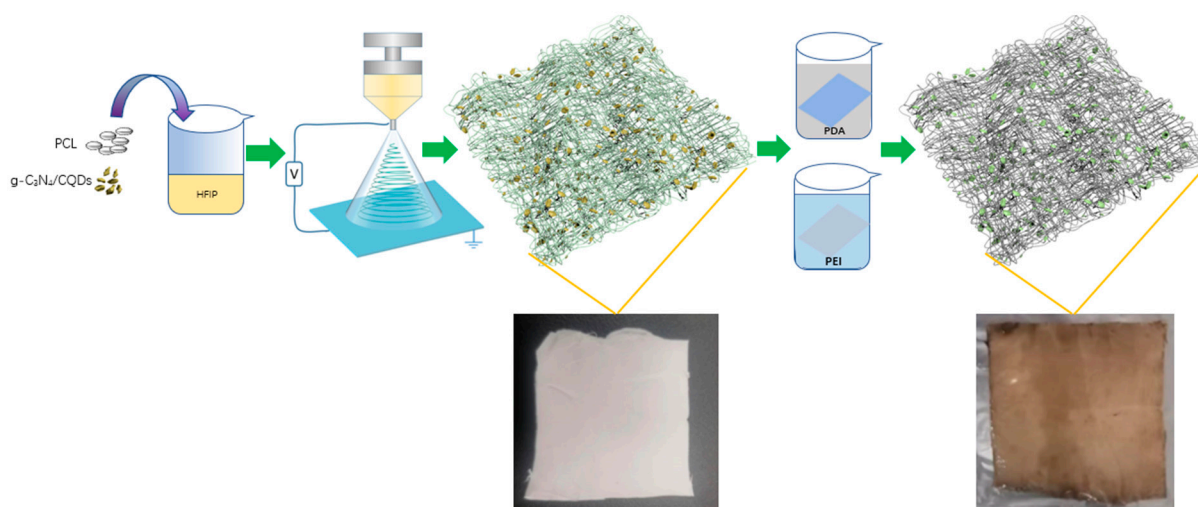


**Figure 1.** The schematic illustration of the fabrication of modified PCL- $g\text{-C}_3\text{N}_4/\text{CQDs}$  electrospun membranes.



Surface modification treatment was a two-step process that combines hydrolysis reaction with subsequent grafting technology, which was briefly described as follows. First, immersed the PCL-g-C<sub>3</sub>N<sub>4</sub>/CQDs electrospun membranes in 2 g·L<sup>−1</sup> DA hydrochloride solution (Tris-HCl buffer, pH = 8.5) at 45 °C with 120 r·min<sup>−1</sup> agitations to form PDA layer for 12 h. Second, placed the washed PDA-coated PCL-g-C<sub>3</sub>N<sub>4</sub>/CQDs electrospun membranes by deionized water in 2 g·L<sup>−1</sup> PEI aqueous solution at 45 °C with 120 r·min<sup>−1</sup> agitations for 12 h. Finally, the modified PCL-g-C<sub>3</sub>N<sub>4</sub>/CQDs electrospun membranes were obtained after washing and drying treatment.

Pristine PCL electrospun membranes, modified PCL electrospun membranes and PCL-g-C<sub>3</sub>N<sub>4</sub>/CQDs electrospun membranes were prepared in a similar manner, respectively.

#### 2.4. Membranes Characterization

The morphologies of the pristine PCL electrospun membranes, modified PCL electrospun membranes, PCL-g-C<sub>3</sub>N<sub>4</sub>/CQDs electrospun membranes and modified PCL-g-C<sub>3</sub>N<sub>4</sub>/CQDs electrospun membranes were observed using scanning electron microscopy (SEM, ZEISS Sigma, Germany) and the microstructures of g-C<sub>3</sub>N<sub>4</sub>/CQDs composites were observed by transmission electron microscopy (TEM, JEM-2100F). The UV-vis absorption spectra and photoluminescence of g-C<sub>3</sub>N<sub>4</sub>/CQDs composites were measured with a UV-vis-NIR double beam spectrophotometer (Lambda 1050, Perkin-Elmer, Waltham, MA, USA) and a steady-state/transient fluorescence spectrometer (Edinburgh Instruments, Livingston FL1000, UK). X-ray diffraction (XRD) patterns were obtained with an x-ray diffractometer (XRD, MiniFlex 600, Rigaku, The Woodlands, TX, USA) at a scanning speed of 2°/min. Fourier-transformed infrared (FTIR) spectra were analyzed on a fourier infrared spectrometer (Vector-22, BRUKER, wavenumber region: 500~4000 cm<sup>−1</sup>, wavenumber resolution: 1 cm<sup>−1</sup>). High-resolution XPS spectra were analyzed using an X-ray photoelectron spectrometer (NexsaG2, Thermo Scientific, Waltham, Ma, USA, voltage: 12 kV, energy range: 100~700 eV, scanning step: 0.05 eV).

#### 2.5. Photocatalytic Degradation Experiment

The adsorption experiments were performed at room temperature in the dark by immersing 0.05 g of pristine PCL electrospun membranes, modified PCL electrospun membranes, PCL-g-C<sub>3</sub>N<sub>4</sub>/CQDs electrospun membranes and modified PCL-g-C<sub>3</sub>N<sub>4</sub>/CQDs electrospun membranes into 50 mL of AFB<sub>1</sub> aqueous solutions (0.5 µg/mL), respectively. During the experiments, 0.5 mL of the AFB<sub>1</sub> aqueous solution was taken every 5 min within 30 min.

The adsorption-photocatalysis experiments were performed under visible light radiation, whereas the other concentrations were kept constant with adsorption experiments. A 300 W xenon lamp with a 400 nm cut-off filter was used as a light source. The distance between the Xenon lamp and the AFB<sub>1</sub> aqueous surface was 10 cm. During the experiments, 0.5 mL of the AFB<sub>1</sub> aqueous solution was taken every 5 min for a total of 30 min.

In this study, the concentrations of the AFB<sub>1</sub> were analyzed by the Waters-600 high-performance liquid chromatography (HPLC) equipped with a UV/Visible detector (emission wavelength at 365 nm) and C-18 Phenomenex reverse phase column (250 × 4.6 mm i.d., 5 µm) at a flow rate of 1 mL/min with an isocratic system composed of acetonitrile: methanol: water (10:20:70). The total running time was 20 min and the injection volume was 10 µL.

The stability of the modified PCL-g-C<sub>3</sub>N<sub>4</sub>/CQDs electrospun membranes was evaluated by 5 continuous cycle experiments. NaCl (0.1 mol) and urea (0.1 mol) were added into AFB<sub>1</sub> solutions in the dark, respectively, before adsorption experiments as electrostatic and hydrogen bond inhibitors to explore the adsorption mechanism of AFB<sub>1</sub>. In order to understand the mechanism of photodegradation of AFB<sub>1</sub> by the electrospun membranes, active species trapping experiments were carried out with the addition of ammonium oxalate (AO, 1 mM), isopropanol (IPA, 1 mM), and 1,4-benzoquinone (BQ, 1 mM) to capture photogenerated holes (h<sup>+</sup>), hydroxyl radicals (•OH) and super-oxide anion radicals (•O<sub>2</sub><sup>−</sup>), respectively.

### 3. Results and Discussion

#### 3.1. Micro-Structure of PCL-g-C<sub>3</sub>N<sub>4</sub>/CQDs Electrospun Membranes

The morphologies of the pristine PCL electrospun membranes, modified PCL electrospun membranes, PCL-g-C<sub>3</sub>N<sub>4</sub>/CQDs electrospun membranes and modified PCL-g-C<sub>3</sub>N<sub>4</sub>/CQDs electrospun membranes were displayed in Figure 2. Figure 2a presented the SEM images of the pristine PCL electrospun membranes, and these smooth PCL nanofibers with a diameter around of 1200 nm form a crosslink network structure. After surface modification treatment (PDA/PEI-coating) the color of the pristine PCL electrospun membranes changed from white to dark grey, and some randomly distributed small bumps could be observed on the surface of the modified PCL electrospun membranes as depicted in Figure 2b. When g-C<sub>3</sub>N<sub>4</sub>/CQDs composites were dissolved in the PCL electrospun solution, the synthesized PCL-g-C<sub>3</sub>N<sub>4</sub>/CQDs electrospun nanofibers could still retain crosslink network structure, and a specific amount of embedded g-C<sub>3</sub>N<sub>4</sub>/CQDs could be observed in Figure 2c. Similar to the pristine PCL electrospun membranes after surface modification treatment, small bumps which adhere to the surface of PCL nanofibers and exposed g-C<sub>3</sub>N<sub>4</sub>/CQDs composites also could be observed in the modified PCL-g-C<sub>3</sub>N<sub>4</sub>/CQDs electrospun membranes as shown in Figure 2d. Compared with PCL-g-C<sub>3</sub>N<sub>4</sub>/CQDs electrospun membranes, the surface modification by PDA/PEI was conducive for the adsorption of AFB<sub>1</sub> to the vicinity of photodegradation sites and promoting the contact probability of AFB<sub>1</sub> and g-C<sub>3</sub>N<sub>4</sub>/CQDs composites, which improves the photocatalytic efficiency.

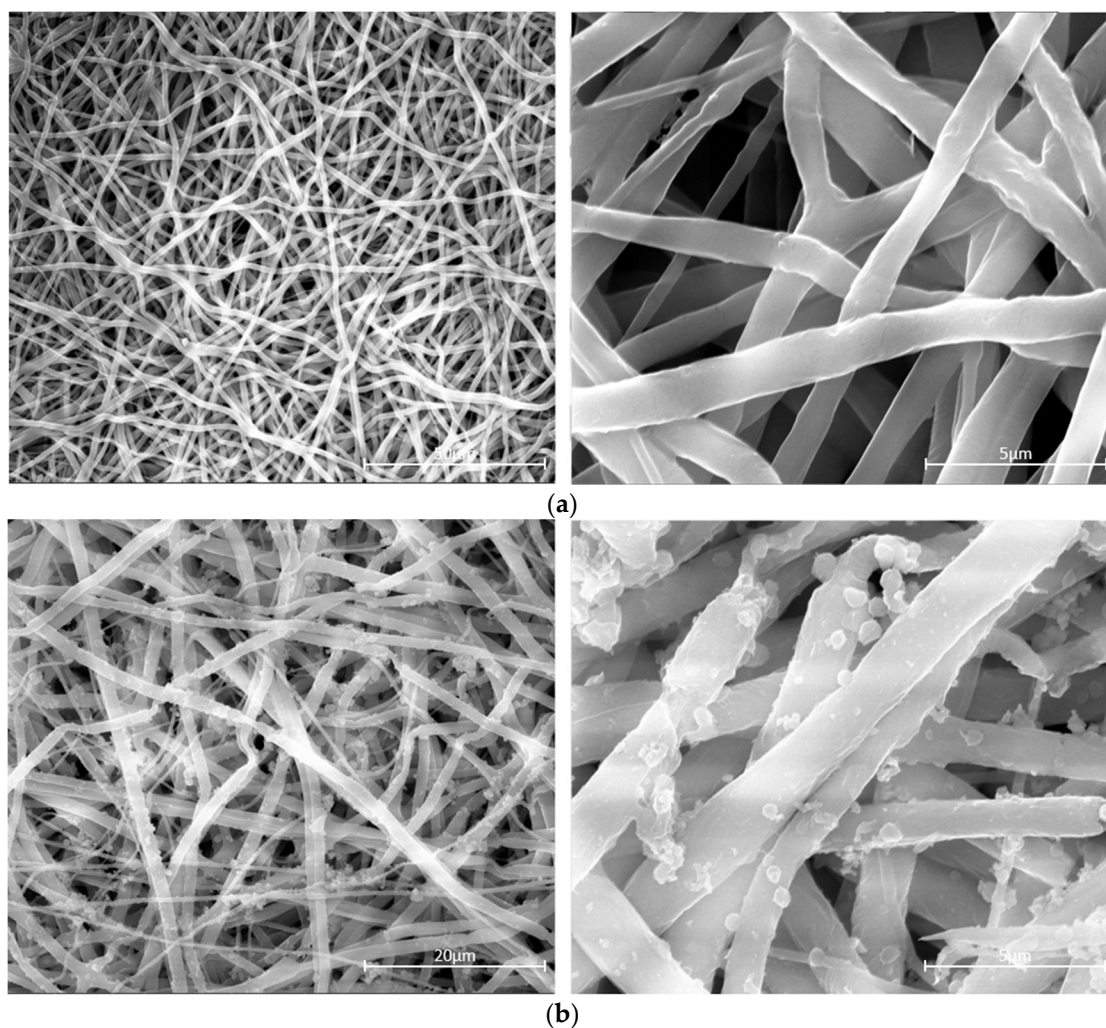
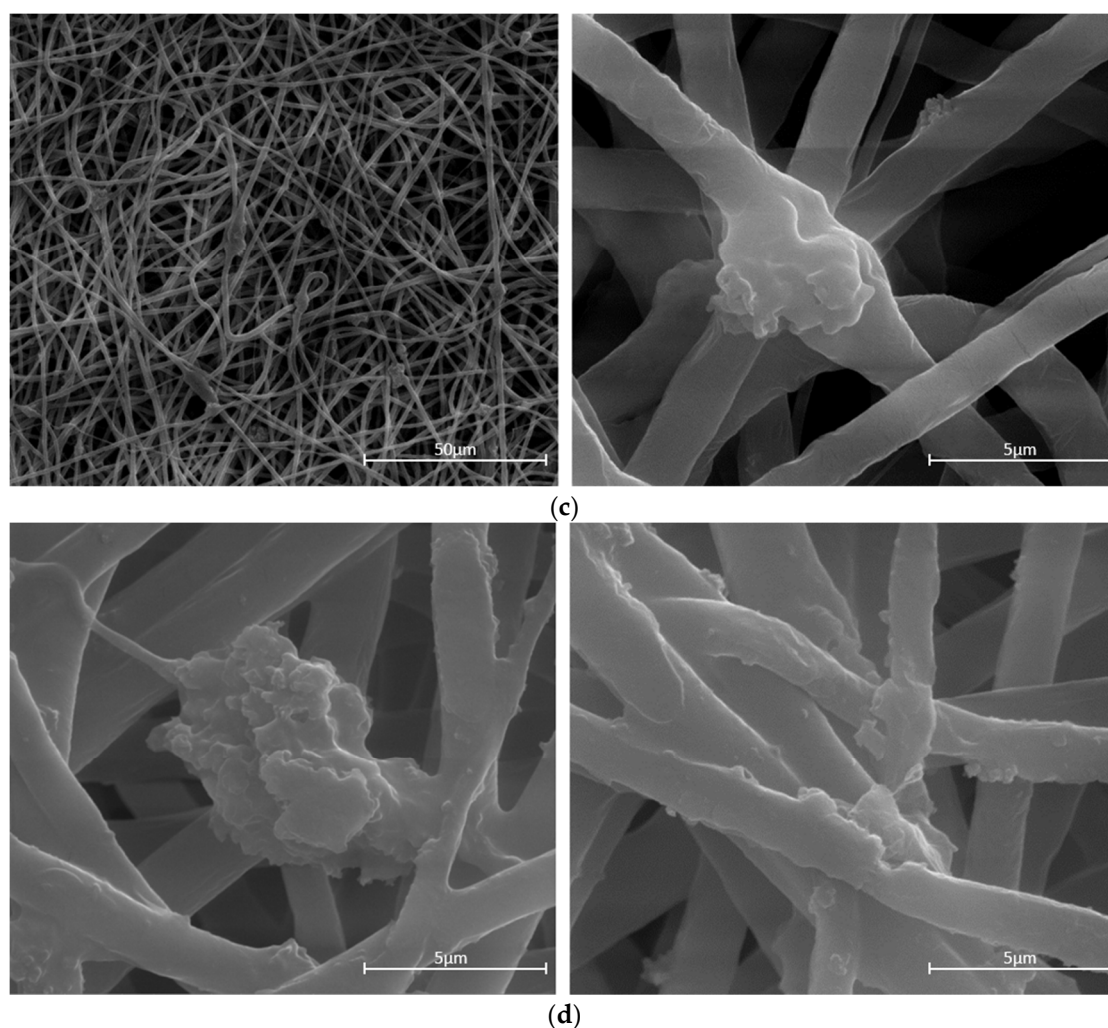


Figure 2. Cont.



**Figure 2.** SEM images of (a) pristine PCL electrospun membranes, (b) modified PCL electrospun membranes, (c) PCL-g-C<sub>3</sub>N<sub>4</sub>/CQDs electrospun membranes, and (d) modified PCL-g-C<sub>3</sub>N<sub>4</sub>/CQDs electrospun membranes.

### 3.2. Micro-Structure of g-C<sub>3</sub>N<sub>4</sub>/CQDs Composites

Figure 3 showed the TEM and HRTEM images of g-C<sub>3</sub>N<sub>4</sub>/CQDs composites, revealing the detailed microstructure. Apparently, many CQDs with diameters of 10–20 nm were uniformly decorated on g-C<sub>3</sub>N<sub>4</sub> with numerous stacked block structures, which was consistent with the findings from previous studies [40,41]. In addition, a sharp dividing line in the HRTEM image further exhibited the coexistence of g-C<sub>3</sub>N<sub>4</sub> and CQDs nanoparticles, which confirmed that CQDs homogeneously combined with g-C<sub>3</sub>N<sub>4</sub>. The micro-regional heterostructures between CQDs and g-C<sub>3</sub>N<sub>4</sub> could effectively enhance different orientation intrinsic driving forces to accelerate the separation and transfer of photogenerated charges [42].

### 3.3. UV-vis Absorption Spectra and PL Spectra of g-C<sub>3</sub>N<sub>4</sub> with Different Content of CQDs

To analyze the light capture ability of g-C<sub>3</sub>N<sub>4</sub>/CQD composites, UV-vis absorption spectra of g-C<sub>3</sub>N<sub>4</sub>/CQDs composites with different contents of CQDs (0.1%, 0.3%, 0.5%, and 0.7%) and pristine g-C<sub>3</sub>N<sub>4</sub> were recorded, as shown in Figure 4a. Compared with pristine g-C<sub>3</sub>N<sub>4</sub>, the light absorption region of g-C<sub>3</sub>N<sub>4</sub>/CQDs was greatly enhanced with the increasing content of CQDs. Redshift was observed from the absorption edge of g-C<sub>3</sub>N<sub>4</sub> at 463 nm, which may be due to the effective combination of CQDs into g-C<sub>3</sub>N<sub>4</sub> by thermal polymerization. We performed photoluminescence (PL) analysis, the results were shown in Figure 4b, to study the recombination of photogenerated charges of g-C<sub>3</sub>N<sub>4</sub>/CQDs com-



posites using an excitation wavelength of 360 nm. Both pristine g-C<sub>3</sub>N<sub>4</sub> and g-C<sub>3</sub>N<sub>4</sub>/CQDs samples with different contents of CQDs (0.1%, 0.3%, 0.5%, and 0.7%) had emission peaks at about 460 nm originated from inter-band recombination of photogenerated charges. The implanted CQDs acted as electron-accepting and transport centers that could facilitate the photogenerated charges transfer greatly and promote  $\pi$ -electron delocalization in the micro-region, inhibiting the recombination of photogenerated charges. Thereby, the emission peaks dramatically decreased with the increase in CQDs content (0~0.5%) and the photocatalytic efficiency was improved accordingly [38]. However, when the content of CQDs raised to 0.7%, the PL emission intensity turned over. In this situation, excess CQDs not only weakened the light absorption of g-C<sub>3</sub>N<sub>4</sub>, but also acted as the recombination sites of photogenerated charges, leading to an increase in emission intensity and a decrease in photocatalytic efficiency [40].

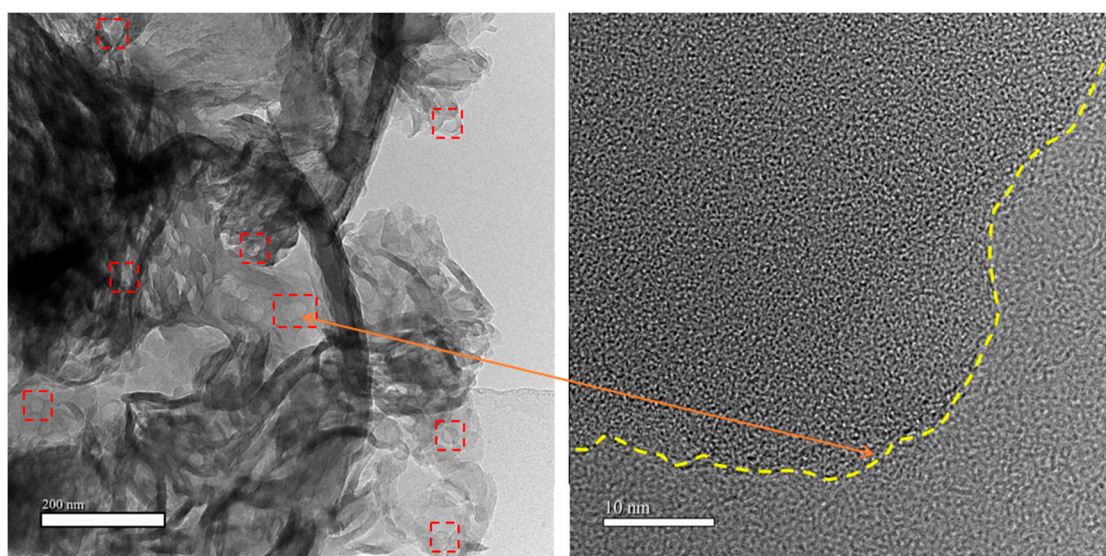


**Figure 3.** TEM and HRTEM images of g-C<sub>3</sub>N<sub>4</sub>/CQD composites.

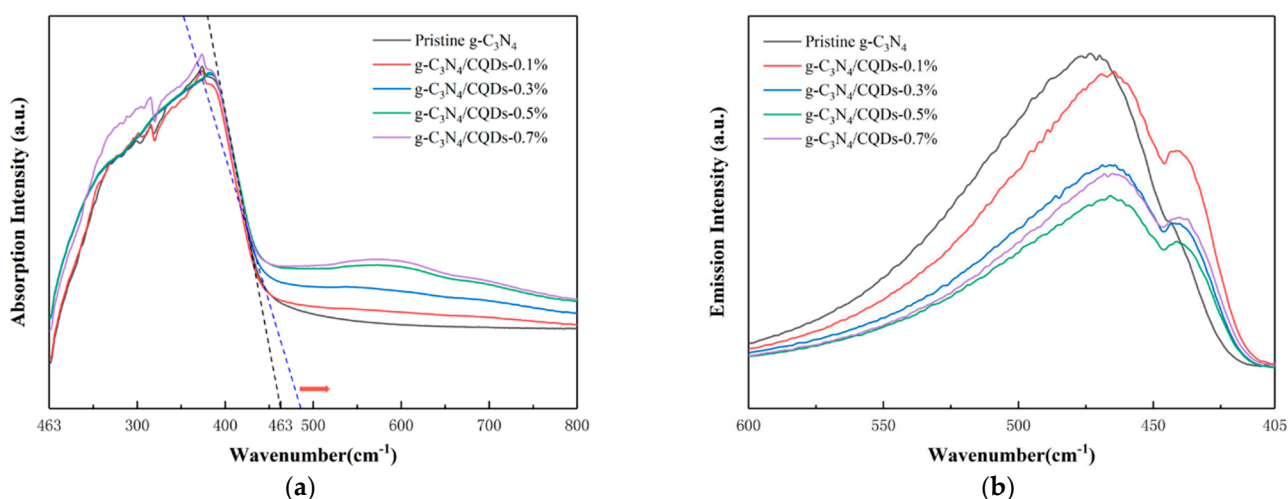


**Figure 4.** (a) UV-vis absorption spectra and (b) PL spectra of g-C<sub>3</sub>N<sub>4</sub> with different content of CQDs from 0~0.7%.

### 3.4. XRD Analysis of the Electrospun Membranes and g-C<sub>3</sub>N<sub>4</sub>/CQDs Composites

Figure 5a showed the XRD patterns of pristine PCL electrospun membranes, modified PCL electrospun membranes, PCL-g-C<sub>3</sub>N<sub>4</sub>/CQDs electrospun membranes and modified PCL-g-C<sub>3</sub>N<sub>4</sub>/CQDs electrospun membranes. The typical diffraction peaks at 21.5° and



23.9° correspond to (110) and (200) crystal planes of PCL, respectively [28]. After surface modification treatment, two accompanying peaks at 22.2° and 24.5° appeared on the XRD patterns of modified PCL electrospun membranes and modified PCL-g-C<sub>3</sub>N<sub>4</sub>/CQDs electrospun membranes, confirming the structural change caused by the functionalization reaction [43]. This also revealed that the structure of PCL has not been destroyed by surface modification treatment as the two diffraction peaks of PCL stay the same in the four XRD patterns. As stated above, XRD patterns showed that those two electrospun membranes were successfully modified. Moreover, no diffraction peaks for g-C<sub>3</sub>N<sub>4</sub>/CQDs were observed due to the low content. The details of XRD patterns of four membranes from 15° to 30° can be seen in Figure S2a. In order to analyze the crystal structure of the synthesized g-C<sub>3</sub>N<sub>4</sub>/CQDs composites, the XRD patterns of g-C<sub>3</sub>N<sub>4</sub>, CQDs and g-C<sub>3</sub>N<sub>4</sub>/CQDs composites were also obtained, as shown in Figure 5b. The characteristic peak of g-C<sub>3</sub>N<sub>4</sub> appears at  $2\theta = 13.1^\circ$  was assigned to the (100) plane, which was attributed to the triazine unit. Additionally, another stronger peak that appears at 27.6° was the typical (002) diffraction plane attributed to the inter-planar stacking of the aromatic system in g-C<sub>3</sub>N<sub>4</sub> [44]. The XRD pattern of the CQDs exhibited a wide bump around 10°, corresponding to the (002) plane [45]. It is worth noting that due to the low content and uniform distribution of the CQDs, almost no diffraction peaks of CQDs were observed in the g-C<sub>3</sub>N<sub>4</sub>/CQDs composite, revealing that the incorporation of CQDs did not significantly change the crystal structure of g-C<sub>3</sub>N<sub>4</sub>. More details can be found in Figure S2b.

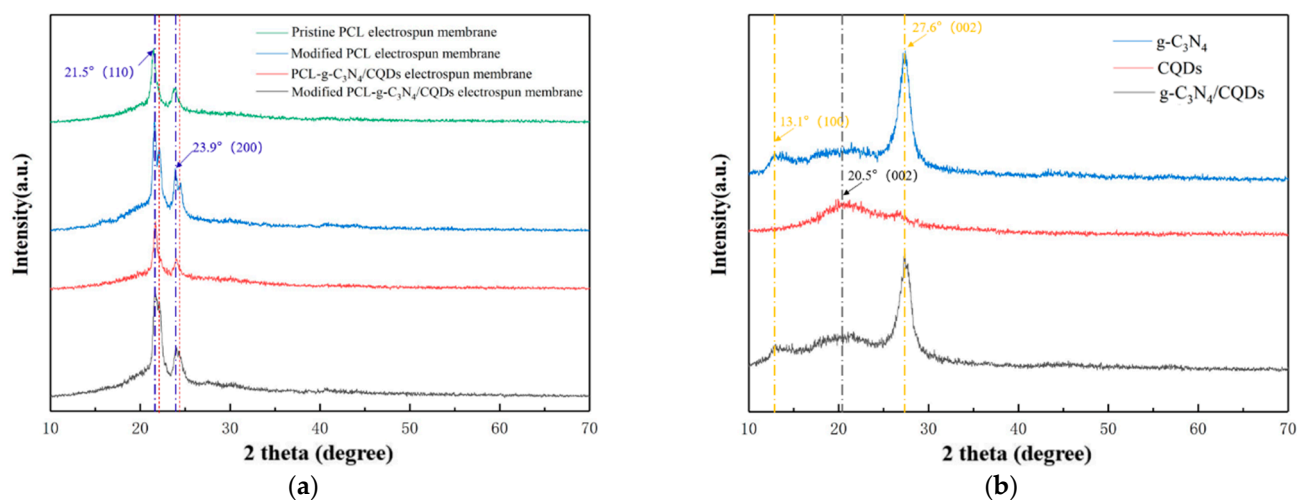


**Figure 5.** XRD patterns of (a) four membranes and (b) g-C<sub>3</sub>N<sub>4</sub>, CQDs, g-C<sub>3</sub>N<sub>4</sub>/CQDs.

### 3.5. XPS Analysis of the Modified Electrospun Membranes

X-ray photoelectron spectroscopy (XPS) was used to investigate the chemical state and composition of the modified PCL-g-C<sub>3</sub>N<sub>4</sub>/CQDs electrospun membranes as shown in Figure S3, which showed that it was completely composed of C, N and O elements. As the content of g-C<sub>3</sub>N<sub>4</sub>/CQDs in those electrospun membranes was low and played a decisive role in the photodegradation of AFB<sub>1</sub>, we further carried out XPS analysis on g-C<sub>3</sub>N<sub>4</sub>/CQDs composites. The XPS wide scan spectra of g-C<sub>3</sub>N<sub>4</sub>/CQDs was shown in Figure 6a, revealing the existence of C, N and O elements at binding energies of 288 (C 1s), 400 (N 1s) and 532 eV (O 1s). Further, we used the peak-splitting simulation method to understand the chemical properties. In the high-resolution XPS spectra of C 1s (Figure 6b), four peaks located at 285.1, 286.0, 288.7 and 294.1 eV were ascribed to graphitic carbon (C=C) of CQDs, a small quantity of C-O species, sp<sup>2</sup> hybridized carbon (N-C=N) of g-C<sub>3</sub>N<sub>4</sub> and  $\pi$ -excitation, respectively [42,46]. The spectra of N 1s (Figure 6c) could be fitted into four peaks at 398.9, 399.8, 401.2 and 404.5 eV, which could be assigned to sp<sup>2</sup> hybridized aromatic N (C-N=C) in triazine rings, tertiary N in N-(C)<sub>3</sub> and amino groups (N-H),  $\pi$ -excitation, respectively [40,47]. The spectra of O 1s (Figure 6d) could be fitted into two

peaks at 531.7 and 533.4 eV, which could be assigned to C-O and O-H of lattice oxygen and adsorbed water, respectively [42,46]. In the whole spectrum, no characteristic peak related to any other element was observed both in modified PCL-g-C<sub>3</sub>N<sub>4</sub>/CQDs electrospun membranes and g-C<sub>3</sub>N<sub>4</sub>/CQDs composites indicating this metal-free material can avoid the release of poisonous metal ions during practical application.

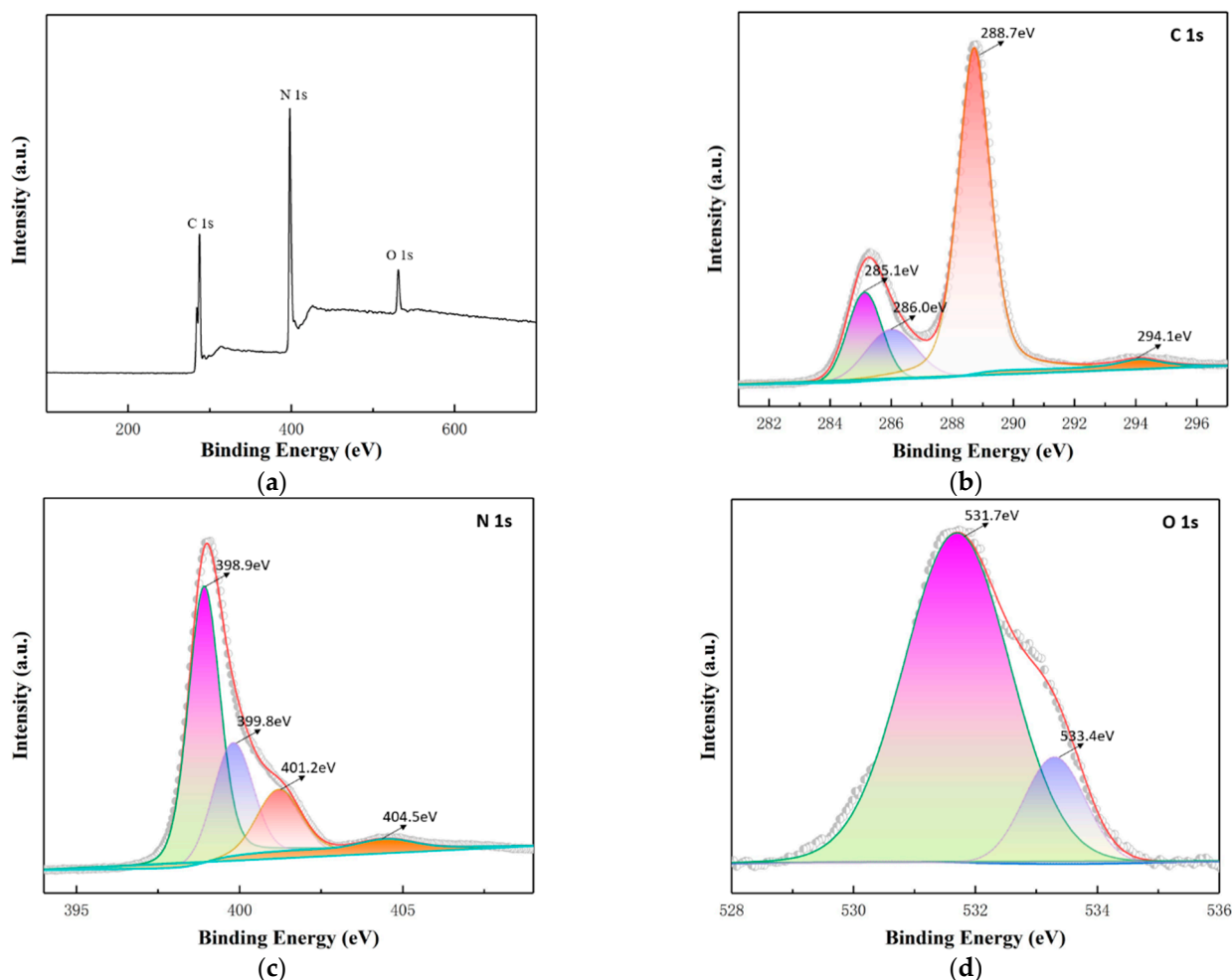


**Figure 6.** XPS survey spectrum of g-C<sub>3</sub>N<sub>4</sub>/CQDs composites: (a) the full-scale XPS spectrum, high-resolution XPS spectra of (b) C 1s, (c) N 1s, (d) O 1s.

### 3.6. FTIR Analysis of the Electrospun Membranes and g-C<sub>3</sub>N<sub>4</sub>/CQDs Composites

Fourier transform infrared spectra (FTIR) can be used to characterize electrospun membranes and g-C<sub>3</sub>N<sub>4</sub>/CQDs composites. Figure 7a showed the FTIR spectra of the four membranes, which were almost the same. The PCL-related absorption peaks were observed at 2949 cm<sup>-1</sup> (asymmetric -CH<sub>2</sub>- stretching), 2868 cm<sup>-1</sup> (symmetric -CH<sub>2</sub>- stretching), 1727 cm<sup>-1</sup> (-C=O carbonyl stretching), 1293 cm<sup>-1</sup> (C-O and C-C stretching in the crystalline phase), 1240 cm<sup>-1</sup> (asymmetric C-O stretching), 1190 cm<sup>-1</sup> (symmetric C-O stretching), and 1157 cm<sup>-1</sup> (C-O and C-C stretching in the crystalline phase) [48,49]. Whether the electrospun membranes were surface-modified or anchored with g-C<sub>3</sub>N<sub>4</sub>/CQDs composites, their FTIR results were basically the same. The reason may be that the PDA/PEI molecules and g-C<sub>3</sub>N<sub>4</sub>/CQDs composites were too few to detect. The same was true of the work of other researchers, such as Scaffaro et al. [49], and Xu et al. [50]. Figure 7b showed the FTIR spectra of the g-C<sub>3</sub>N<sub>4</sub> and g-C<sub>3</sub>N<sub>4</sub>/CQDs composites. The main absorption peaks at 3200 cm<sup>-1</sup> (N-H stretching), 1637 cm<sup>-1</sup> (C=N stretching), 1574 cm<sup>-1</sup> (C=N stretching), 1405 cm<sup>-1</sup> (C-N stretching), 1316 cm<sup>-1</sup> (C-N stretching), 1236 cm<sup>-1</sup> (C-N stretching), and 810 cm<sup>-1</sup> (vibration mode of 3-s-triazine unit) belonged to g-C<sub>3</sub>N<sub>4</sub> [40,47]. It was clear that the g-C<sub>3</sub>N<sub>4</sub> and

$g\text{-C}_3\text{N}_4/\text{CQDs}$  composites had almost the same FTIR spectra, indicating that the introduction of CQDs did not significantly change the chemical structure of  $g\text{-C}_3\text{N}_4$ .

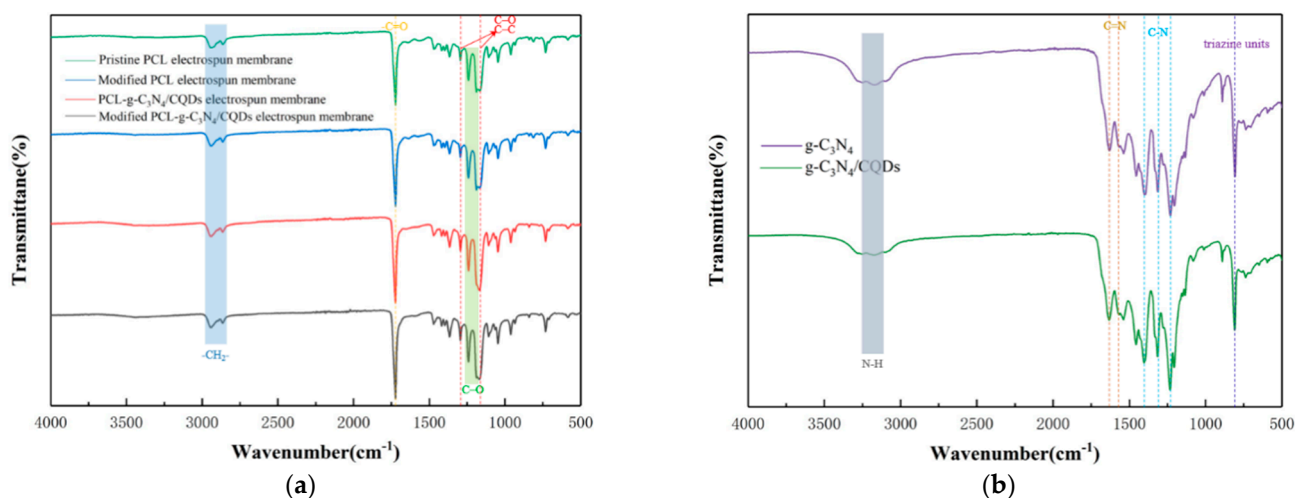


**Figure 7.** FTIR spectra of (a) the as-prepared membranes and (b)  $g\text{-C}_3\text{N}_4$ ,  $g\text{-C}_3\text{N}_4/\text{CQDs}$  composites.

### 3.7. Performance of Removing $\text{AFB}_1$

The adsorption-removal performances of  $\text{AFB}_1$  aqueous solution were evaluated in dark and the adsorption experiments were 30 min. We could see from Figure 8a that the concentrations of  $\text{AFB}_1$  were reduced to 87.1% and 84.2% with pristine PCL electrospun membranes and PCL- $g\text{-C}_3\text{N}_4/\text{CQDs}$  electrospun membranes immersed in 30 min, respectively. However, the adsorption-removal efficiencies were significantly improved and up to 63.5% and 58.6% when using modified PCL electrospun membranes and modified PCL- $g\text{-C}_3\text{N}_4/\text{CQDs}$  electrospun membranes. It could be inferred that the surface modification by PDA/PEI coating not only improved the hydrophilicity of the membranes (Figure S4) but also endowed the membranes with extremely strong adsorption capacity for  $\text{AFB}_1$ . Moreover, we saw that the hydrophobic interaction between the modified membranes and  $\text{AFB}_1$  was a key factor for the adsorption mechanism. The HPLC chromatogram of  $\text{AFB}_1$  aqueous solution concentrations over the adsorption time with modified PCL- $g\text{-C}_3\text{N}_4/\text{CQDs}$  electrospun membranes was demonstrated in Figure 8b. When the experiments were carried out under visible light irradiation, the concentrations of  $\text{AFB}_1$  decreased rapidly with PCL- $g\text{-C}_3\text{N}_4/\text{CQDs}$  electrospun membranes and modified PCL- $g\text{-C}_3\text{N}_4/\text{CQDs}$  electrospun membranes immersed. After 30 min of visible light radiation, only 16.1% and 3.1% of  $\text{AFB}_1$  were left over, as shown in Figure 8c. Moreover, the removal efficiencies of the other two membranes without  $g\text{-C}_3\text{N}_4/\text{CQDs}$  remained almost unchanged compared with the adsorption experiments. These results unambiguously showed that the removal of  $\text{AFB}_1$  under visible light irradiation was due to synergistic adsorption and photocatalytic degradation. The HPLC chromatogram of  $\text{AFB}_1$  aqueous solution concentrations over the irradiation time with modified PCL- $g\text{-C}_3\text{N}_4/\text{CQDs}$  electrospun membranes was demonstrated in Figure 8d. Different from adsorption experiments, intermediate products would be produced during the process of photocatalysis, depending on the type of photocatalysts and reaction conditions [51]. The chromatogram peaks appearing at 8.5–9.5 min in Figure 8d were attributed to intermediate products [51], and most of them were eliminated by adsorption and photocatalysis.

To understand more about the adsorption behavior, the pseudo-first-order [Equation (1)] and pseudo-second-order [Equation (2)] kinetic models were then used to analyze the adsorption kinetics process [12,52].

$$\log(q_e - q_t) = \log q_e - k_1 t / 2.303 \quad (1)$$

$$t/q_t = 1/k_2 q_e^2 + t/q_e \quad (2)$$

where  $q_e$  and  $q_t$  ( $\mu\text{g}/\text{mg}$ ) represent the equilibrium adsorption amount and the adsorption amount at time  $t$ ;  $k_1$  (1/min) and  $k_2$  ( $\text{mg}/(\mu\text{g}\cdot\text{min})$ ) are the rate constants for the first- and second-order adsorption process, respectively. The fitting results were illustrated in Figure 9. The relevant kinetic parameters calculated from the fitting curves were listed in Table 1. In general, the pseudo-first-order model assumes that the adsorption process is mainly due to physical adsorption, whereas the pseudo-second-order model indicates that the whole adsorption process is dominated by chemical adsorption. Both instances of  $R^2$  in the pseudo-first-order model (0.99236) and pseudo-second-order model (0.98694) were greater than 0.95, indicating that physical adsorption and chemical adsorption both contributed to the removal of AFB<sub>1</sub> and exhibited mainly physical adsorption accompanied by chemical adsorption [53].

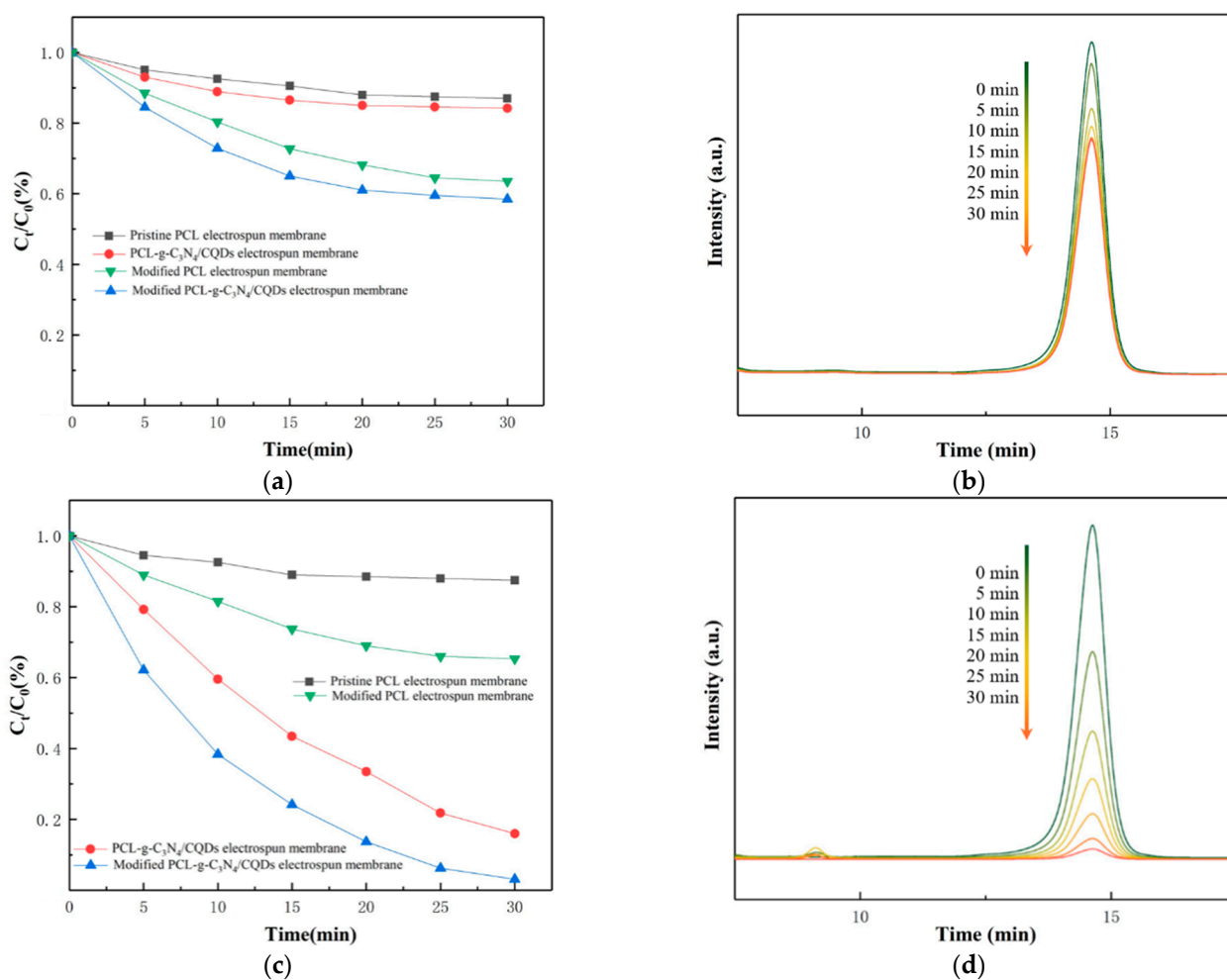


**Figure 8.** (a) Adsorption-removal performances of AFB<sub>1</sub> with the four kinds of membranes under dark. (b) HPLC chromatogram of AFB<sub>1</sub> adsorption-removal with modified PCL-g-C<sub>3</sub>N<sub>4</sub>/CQDs electrospun membranes under dark at different times. (c) Synergistic adsorption and photocatalytic degradation performance of AFB<sub>1</sub> with the four kinds of membranes under visible light irradiation. (d) HPLC chromatogram of AFB<sub>1</sub> adsorption and photocatalytic degradation with modified PCL-g-C<sub>3</sub>N<sub>4</sub>/CQDs electrospun membranes under visible light irradiation at different times.



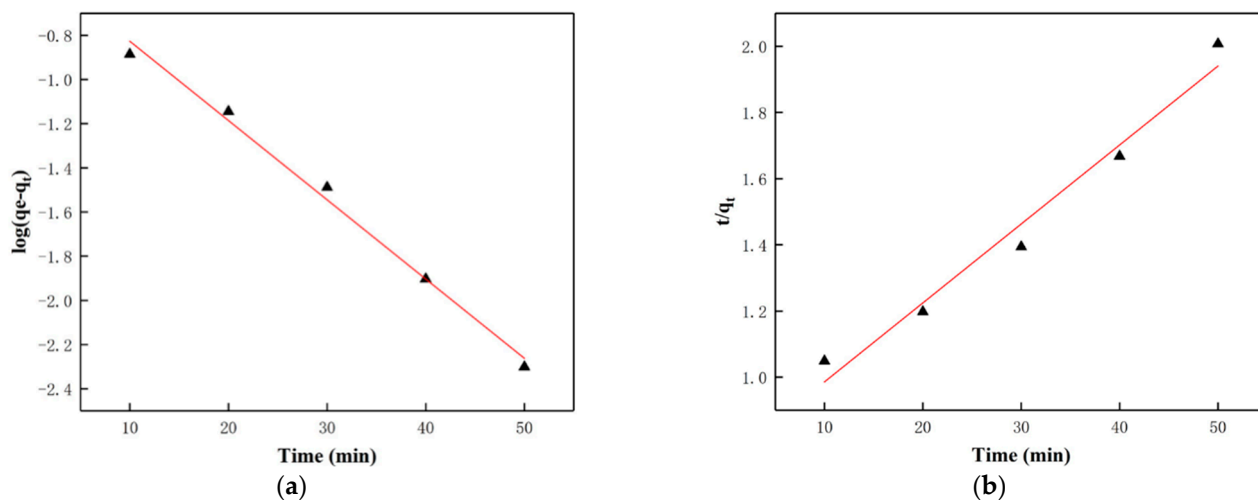


**Figure 9.** Corresponding linear fitting of AFB<sub>1</sub> adsorption by the modified PCL-g-C<sub>3</sub>N<sub>4</sub>/CQDs electrospun membranes with time, (a) pseudo-first-order model and (b) pseudo-second-order model.

**Table 1.** Kinetics parameters for AFB<sub>1</sub> adsorption removal.

Sample	$q_e$ (μg/mg)	Pseudo-First Order $\log(q_e - q_t) = \log q_e - k_1 t / 2.303$		Pseudo-Second Order $t/q_t = 1/k_2 q_e^2 + t/q_e$	
		$k_1$ (1/min)	$R^2$	$k_2$ (mg/(μg·min))	$R^2$
Modified PCL-g-C <sub>3</sub> N <sub>4</sub> /CQDs electrospun membranes	0.2075	0.03589	0.99236	0.02378	0.98694

To test the stability of the modified PCL-g-C<sub>3</sub>N<sub>4</sub>/CQDs electrospun membranes, we conducted 5 consecutive experiments under the same experimental conditions. Figure 10 showed the reproducibility results of AFB<sub>1</sub> degradation. We can learn that the degradation rate reached more than 96% within 30 min after five consecutive experiments. The recyclability of the modified PCL-g-C<sub>3</sub>N<sub>4</sub>/CQDs electrospun membranes shows the possibility of its practical application as well as better economic benefits.

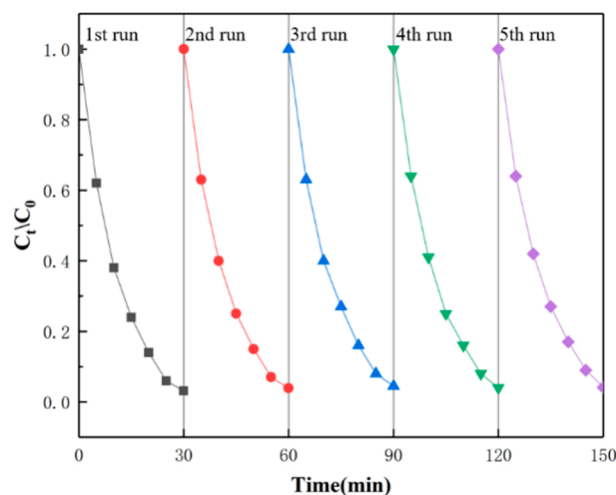


**Figure 10.** The reproducibility of the modified PCL-g-C<sub>3</sub>N<sub>4</sub>/CQDs electrospun membranes for degradation of AFB<sub>1</sub> for 5 cycles.

### 3.8. Mechanism for Enhanced Degradation Performance

To better understand the mechanism of synergistic adsorption and photocatalytic degradation for AFB<sub>1</sub> by the modified PCL-g-C<sub>3</sub>N<sub>4</sub>/CQDs electrospun membranes, modified PCL electrospun membranes and g-C<sub>3</sub>N<sub>4</sub>/CQDs composites were used for adsorption and photocatalysis experiments, respectively, under the same conditions described above. NaCl and urea were added into AFB<sub>1</sub> solutions before adsorption experiments, and the AFB<sub>1</sub> removal rate decreased to 41.3% and 7.31%, as shown in Figure 11a. NaCl and urea are well-known “killers” of electrostatic and hydrogen bonds [54], which indicated that electrostatic attraction and hydrogen bonds were the main adsorption mechanisms between AFB<sub>1</sub> molecules and PDA/PEI coating. For the photocatalysis experiments, AO, IPA and BQ were employed as the scavengers for h<sup>+</sup>, •OH and •O<sub>2</sub><sup>−</sup>, respectively [55]. Figure 11b displays that the degradation rate of the AFB<sub>1</sub> solution without a sacrificial agent was 97.2% after 5 min of visible light irradiation, whereas those with scavengers such as IPA, BQ, and AO were 79.6%, 4.6%, and 96.7%, respectively. Based on the above results, we learned that both •O<sub>2</sub><sup>−</sup> and •OH contributed to AFB<sub>1</sub> degradation, and •O<sub>2</sub><sup>−</sup> played the dominant role.

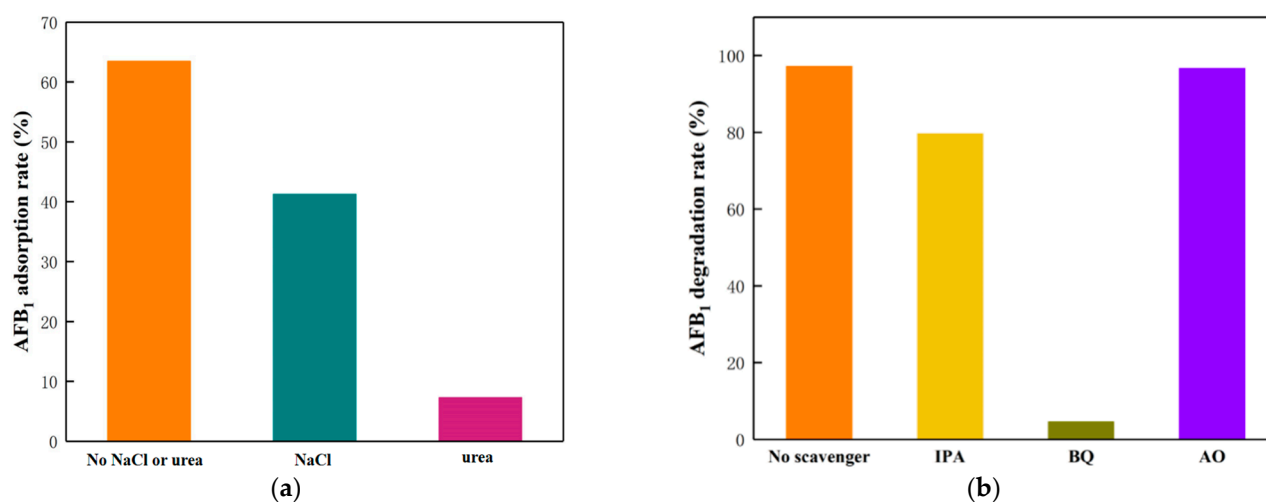


**Figure 11.** (a) Adsorption activities of modified PCL electrospun membranes in the presence of NaCl/urea (or not). (b) Photocatalytic activities of g-C<sub>3</sub>N<sub>4</sub>/CQDs composites for the degradation of AFB<sub>1</sub> in the presence of different scavengers.

The possible adsorption and photocatalytic mechanism of AFB<sub>1</sub> degradation by the modified PCL-g-C<sub>3</sub>N<sub>4</sub>/CQDs electrospun membranes was proposed, as shown in Figure 12. PDA/PEI coating on the surface of the membranes adsorbs and intercepts AFB<sub>1</sub> molecules depending on electrostatic attraction and hydrogen bonds firstly. Upon visible light irradiation, photogenerated electron-hole pairs are generated in the g-C<sub>3</sub>N<sub>4</sub> component of the g-C<sub>3</sub>N<sub>4</sub>/CQDs composites on the membranes. The generated h<sup>+</sup> stayed in the valence band of g-C<sub>3</sub>N<sub>4</sub>, whereas e<sup>−</sup> migrates to the conduction band. As the valence band of g-C<sub>3</sub>N<sub>4</sub> is more negative than the potential of E(OH<sup>−</sup>/•OH) or E(H<sub>2</sub>O/•OH) (1.53V < 1.99 or 2.4V) [40], the h<sup>+</sup> would not react with H<sub>2</sub>O/OH<sup>−</sup> to produce •OH. Moreover, the implanted CQDs act as electron-accepting and transport centers enhance the separation of photogenerated electron-hole pairs and promote the generation of •O<sub>2</sub><sup>−</sup> [56]. Part of •O<sub>2</sub><sup>−</sup> oxidizes H<sub>2</sub>O to •OH [40]. At last, the •O<sub>2</sub><sup>−</sup> and •OH can decompose AFB<sub>1</sub> molecules into smaller fragments, even CO<sub>2</sub> and H<sub>2</sub>O. After the reaction, the modified PCL-g-C<sub>3</sub>N<sub>4</sub>/CQDs electrospun membranes are regenerated as the initial, which can be immediately used in a new process without any further treatment.

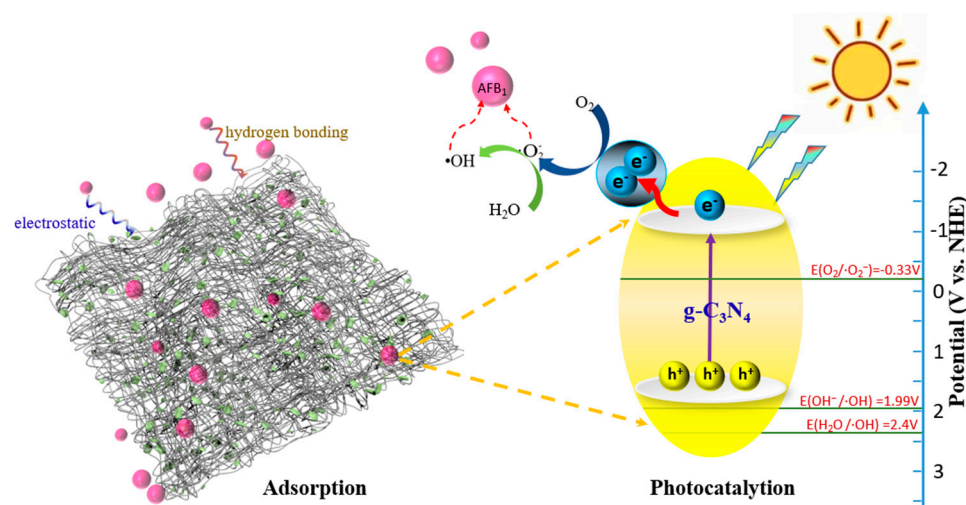


**Figure 12.** The adsorption and photocatalytic mechanism of removal/degradation of AFB<sub>1</sub> for the modified PCL-g-C<sub>3</sub>N<sub>4</sub>/CQDs electrospun membranes.

#### 4. Conclusions

In summary, we employed electrospinning and surface modification technology to prepare novel modified PCL-g-C<sub>3</sub>N<sub>4</sub>/CQDs electrospun membranes. It was observed that adsorption significantly accelerated the process of photodegradation according to contrast experiments. More importantly, the as-prepared membranes can continuously eliminate AFB<sub>1</sub> through the synergistic effects of adsorption and photocatalysis; moreover, regeneration is a green approach synchronized with the reaction under visible light without any physical or chemical treatment. The adsorption mechanism in which electrostatic attraction and hydrogen bonds play major roles was revealed, and the photodegradation mechanism of AFB<sub>1</sub> using g-C<sub>3</sub>N<sub>4</sub>/CQDs composites was studied based on active species trapping experiments. The reusability and stable activity were confirmed during five cycles of degradation experiments. Thus, the novel modified PCL-g-C<sub>3</sub>N<sub>4</sub>/CQDs electrospun membranes demonstrated easy separation, good reusability and provided a new insight into the design of high-performance membranes for the degradation of AFB<sub>1</sub> in practical application.

**Supplementary Materials:** The following supporting information can be downloaded at: <https://www.mdpi.com/article/10.3390/biom13030550/s1>, Figure S1: Photocatalytic degradation of Rhodamine B with different weight ratios of g-C<sub>3</sub>N<sub>4</sub> and CQDs; Figure S2: XRD patterns of (a) four membranes from 15° to 30° and (b) g-C<sub>3</sub>N<sub>4</sub>, CQDs, g-C<sub>3</sub>N<sub>4</sub>/CQDs from 10° to 30°; Figure S3: XPS survey spectrum of the modified PCL-g-C<sub>3</sub>N<sub>4</sub>/CQDs electrospun membrane; Figure S4: Optical images taken while the water droplets come into contact to the surface of (a) pristine PCL electrospun membranes, (b) modified PCL electrospun membranes, (c) PCL-g-C<sub>3</sub>N<sub>4</sub>/CQDs electrospun membranes, and (d) modified PCL-g-C<sub>3</sub>N<sub>4</sub>/CQDs electrospun membranes.

**Author Contributions:** Conceptualization, D.Z. and C.S.; methodology, L.Y.; validation, R.S.; formal analysis, L.Y.; investigation, L.Y.; resources, D.Z. and G.L.; data curation, R.S.; writing—original draft preparation, L.Y.; writing—review and editing, D.Z. and Z.L.; visualization, L.Y.; supervision, D.Z. and H.L.; project administration, D.Z. and S.Z. All authors have read and agreed to the published version of the manuscript.

**Funding:** National Natural Science Foundation of China (62275160).

**Institutional Review Board Statement:** Not applicable.

**Informed Consent Statement:** Not applicable.

**Data Availability Statement:** Raw data are available on request.

**Acknowledgments:** Special thanks to Dengguang Yu from University of Shanghai for Science and Technology. We also thank Wangding at the University of Shanghai for Science and Technology for providing the SEM and TEM measurements used in this study.

**Conflicts of Interest:** The authors declare no conflict of interest. The funders had no role in the design of the study; in the collection, analysis, or interpretation of data; in the writing of the manuscript; or in the decision to publish the results.

## References

1. IARC Working Group on the Evaluation of Carcinogenic Risks to Humans. *Some Traditional Herbal Medicines, Some Mycotoxins, Naphthalene and Styrene*; IEEE: Lyon, France, 2002; Volume 82, pp. 1–556. [\[CrossRef\]](#)
2. European Commission. *Setting Maximum Levels for Certain Contaminants in Foodstuffs*; No 1881; European Commission: Brussels, Belgium, 2006.
3. The State Administration of Market Regulation of China. *GB 2761-2017 Maximum Levels of Mycotoxins in Foods*; The State Administration of Market Regulation of China: Beijing, China, 2017.
4. U.S. Food & Drug Administration. *Compliance Policy Guides-Chapter 5-Food, Colors, and Cosmetics*; U.S. Food & Drug Administration: Washington, DC, USA, 2015.
5. Asghar, M.A.; Ahmed, F.; Jabeen, S.; Bhurgri, M.U.; Asif, H.; Hussain, K. Effects of climatic conditions and hermetic storage on the growth of *Aspergillus parasiticus* and aflatoxin B<sub>1</sub> contamination in basmati rice. *J. Stored Prod. Res.* **2022**, *96*, 101944. [\[CrossRef\]](#)
6. Wang, Y.; Liu, F.; Zhou, X.; Liu, M.; Zang, H.; Liu, X.; Shan, A.; Feng, X. Alleviation of Oral Exposure to Aflatoxin B<sub>1</sub>-Induced Renal Dysfunction, Oxidative Stress, and Cell Apoptosis in Mice Kidney by Curcumin. *Antioxidants* **2022**, *11*, 1082. [\[CrossRef\]](#) [\[PubMed\]](#)
7. Tumukunde, E.; Ma, G.; Li, D.; Yuan, J.; Qin, L.; Wang, S. Current research and prevention of aflatoxins in China. *World Mycotoxin J.* **2020**, *13*, 121–138. [\[CrossRef\]](#)
8. Ma, F.; Cai, X.; Mao, J.; Yu, L.; Li, P. Adsorptive removal of aflatoxin B<sub>1</sub> from vegetable oils via novel adsorbents derived from a metal-organic framework. *J. Hazard. Mater.* **2021**, *412*, 125170. [\[CrossRef\]](#) [\[PubMed\]](#)
9. Wang, M.; Hearon, S.E.; Phillips, T.D. A high capacity bentonite clay for the sorption of aflatoxins. *Food Addit. Contam. Part A* **2020**, *37*, 332–341. [\[CrossRef\]](#) [\[PubMed\]](#)
10. Karmanov, A.P.; Kanarsky, A.V.; Kocheva, L.S.; Semenov, E.I.; Belyy, V.A. In vitro study of adsorption efficiency of natural lignins towards aflatoxin B<sub>2</sub>. *React. Funct. Polym.* **2021**, *167*, 105033. [\[CrossRef\]](#)
11. Raesi, S.; Mohammadi, R.; Khammar, Z.; Paimard, G.; Abdalbeygi, S.; Sarlak, Z.; Rouhi, M. Photocatalytic detoxification of aflatoxin B<sub>1</sub> in an aqueous solution and soymilk using nano metal oxides under UV light: Kinetic and isotherm models. *LWT—Food Sci. Technol.* **2022**, *154*, 112638. [\[CrossRef\]](#)
12. Xu, B.; Wang, X.; Huang, Y.; Liu, J.; Wang, D.; Feng, S.; Huang, X.; Wang, H. Electrospinning preparation of PAN/TiO<sub>2</sub>/PANI hybrid fiber membrane with highly selective adsorption and photocatalytic regeneration properties. *Chem. Eng. J.* **2020**, *399*, 125749. [\[CrossRef\]](#)
13. Matei, E.; Covaliu-Mierla, C.I.; Turcanu, A.A.; Rapa, M.; Predescu, A.M.; Predescu, C. Multifunctional Membranes-A Versatile Approach for Emerging Pollutants Removal. *Membranes* **2022**, *12*, 67. [\[CrossRef\]](#)
14. Kumara, S.; Munaweera, I.; Kottegoda, N. A comprehensive review on electrospun nanohybrid membranes for wastewater treatment. *Beilstein J. Nanotechnol.* **2022**, *13*, 137–159. [\[CrossRef\]](#)
15. Wu, W.; Zhang, X.; Qin, L.; Li, X.; Meng, Q.; Shen, C.; Zhang, G. Enhanced MPBR with polyvinylpyrrolidone-graphene oxide/PVDF hollow fiber membrane for efficient ammonia nitrogen wastewater treatment and high-density *Chlorella* cultivation. *Chem. Eng. J.* **2020**, *379*, 122368. [\[CrossRef\]](#)
16. Lee, H.; Murai, M.; Son, D.; Oh, S.-G.; Kim, M.; Paeng, K.; Kim, I.S. A composite of carbon nanofiber/copper particle-anchored thiol-incorporated silica nanoparticles utilizable for heavy metal adsorption. *Compos. Commun.* **2022**, *34*, 101256. [\[CrossRef\]](#)
17. Byun, S.; Lee, J.; Lee, J.; Jeong, S. Reusable carbon nanotube-embedded polystyrene/polyacrylonitrile nanofibrous sorbent for managing oil spills. *Desalination* **2022**, *537*, 115865. [\[CrossRef\]](#)
18. Yu, D.G.; Li, Q.; Song, W.; Xu, L.; Zhang, K.; Zhou, T. Advanced technique-based combination of innovation education and safety education in higher education. *J. Chem. Edu.* **2023**, *100*, 507–516. [\[CrossRef\]](#)
19. Bai, Y.; Liu, Y.; Lv, H.; Shi, H.; Zhou, W.; Liu, Y.; Yu, D.G. Processes of Electrospun Polyvinylidene Fluoride-Based Nanofibers.; Their Piezoelectric Properties.; and Several Fantastic Applications. *Polymers* **2022**, *14*, 4311. [\[CrossRef\]](#) [\[PubMed\]](#)
20. Zhang, J.; Gao, X.; Guo, W.; Wu, Z.; Yin, Y.; Li, Z. Enhanced photocatalytic activity of TiO<sub>2</sub>/UiO-67 under visible-light for aflatoxin B<sub>1</sub> degradation. *RSC Adv.* **2022**, *12*, 6676–6682. [\[CrossRef\]](#)
21. Dai, K.; Lu, L.; Liang, C.; Liu, Q.; Zhu, G. Heterojunction of facet coupled g-C<sub>3</sub>N<sub>4</sub>/surface-fluorinated TiO<sub>2</sub> nanosheets for organic pollutants degradation under visible LED light irradiation. *Appl. Catal. B Environ.* **2014**, *156–157*, 331–340. [\[CrossRef\]](#)
22. Fujishima, A.; Honda, K. Electrochemical photolysis of water at a semiconductor electrode. *Nature* **1972**, *238*, 37–38. [\[CrossRef\]](#) [\[PubMed\]](#)
23. Kumar, A.; Kumar, A.; Krishnan, V. Perovskite Oxide Based Materials for Energy and Environment-Oriented Photocatalysis. *ACS Catal.* **2020**, *10*, 10253–10315. [\[CrossRef\]](#)



24. Huang, X.; Jiang, W.; Zhou, J.; Yu, D.G.; Liu, H. The Applications of Ferulic-Acid-Loaded Fibrous Films for Fruit Preservation. *Polymers* **2022**, *14*, 4947. [[CrossRef](#)]
25. Liu, H.; Bai, Y.; Huang, C.; Wang, Y.; Ji, Y.; Du, Y.; Xu, L.; Yu, D.-G.; Bligh, S.W.A. Recent Progress of Electrospun Herbal Medicine Nanofibers. *Biomolecules* **2023**, *13*, 184. [[CrossRef](#)] [[PubMed](#)]
26. Eom, J.; Kwak, Y.; Nam, C. Electrospinning fabrication of magnetic nanoparticles-embedded polycaprolactone (PCL) sorbent with enhanced sorption capacity and recovery speed for spilled oil removal. *Chemosphere* **2022**, *303*, 135063. [[CrossRef](#)] [[PubMed](#)]
27. Cao, X.; Chen, W.; Zhao, P.; Yang, Y.; Yu, D.G. Electrospun Porous Nanofibers: Pore-Forming Mechanisms and Applications for Photocatalytic Degradation of Organic Pollutants in Wastewater. *Polymers* **2022**, *14*, 3990. [[CrossRef](#)] [[PubMed](#)]
28. Wang, Z.; Song, X.; Cui, Y.; Cheng, K.; Tian, X.; Dong, M.; Liu, L. Silk fibroin H-fibroin/poly(epsilon-caprolactone) core-shell nanofibers with enhanced mechanical property and long-term drug release. *J. Colloid Interface Sci.* **2021**, *593*, 142–151. [[CrossRef](#)] [[PubMed](#)]
29. Almasian, A.; Jalali, M.L.; Fard, G.C.; Maleknia, L. Surfactant grafted PDA-PAN nanofiber: Optimization of synthesis, characterization and oil absorption property. *Chem. Eng. J.* **2017**, *326*, 1232–1241. [[CrossRef](#)]
30. Zhang, Y.; Guan, J.; Wang, X.; Yu, J.; Ding, B. Balsam-Pear-Skin-Like Porous Polyacrylonitrile Nanofibrous Membranes Grafted with Polyethyleneimine for Postcombustion CO<sub>2</sub> Capture. *ACS Appl. Mater. Interfaces* **2017**, *9*, 41087–41098. [[CrossRef](#)]
31. Zhao, Z.; Zhang, H.; Chen, H.; Xu, Y.; Ma, L.; Wang, Z. An efficient photothermal-chemotherapy platform based on a polyacrylamide/phytic acid/polydopamine hydrogel. *J. Mater. Chem. B* **2022**, *10*, 4012–4019. [[CrossRef](#)]
32. Cao, S.; Low, J.; Yu, J.; Jaroniec, M. Polymeric Photocatalysts Based on Graphitic Carbon Nitride. *Adv. Mater.* **2015**, *27*, 2150–2176. [[CrossRef](#)]
33. Jiang, L.; Yuan, X.; Pan, Y.; Liang, J.; Zeng, G.; Wu, Z.; Wang, H. Doping of graphitic carbon nitride for photocatalysis: A review. *Appl. Catal. B Environ.* **2017**, *217*, 388–406. [[CrossRef](#)]
34. Yu, X.; Su, H.; Zou, J.; Liu, Q.; Wang, L.; Tang, H. Doping-induced metal-N active sites and bandgap engineering in graphitic carbon nitride for enhancing photocatalytic H<sub>2</sub> evolution performance. *Chin. J. Catal.* **2022**, *43*, 421–432. [[CrossRef](#)]
35. Wang, H.; Thangamuthu, M.; Wu, Z.; Yang, J.; Yuan, H.; Tang, J. Self-assembled sulphur doped carbon nitride for photocatalytic water reforming of methanol. *Chem. Eng. J.* **2022**, *445*, 136790. [[CrossRef](#)]
36. Tang, S.; Yang, S.; Chen, Y.; Yang, Y.; Li, Z.; Zi, L.; Liu, Y.; Wang, Y.; Li, Z.; Fu, Z.; et al. Ionothermally synthesized S-scheme isotype heterojunction of carbon nitride with significantly enhanced photocatalytic performance for hydrogen evolution and carbon dioxide reduction. *Carbon* **2023**, *201*, 815–828. [[CrossRef](#)]
37. Gao, W.; Zhang, S.; Wang, G.; Cui, J.; Lu, Y.; Rong, X.; Gao, C. A review on mechanism, applications and influencing factors of carbon quantum dots based photocatalysis. *Ceram. Int.* **2022**, *48*, 35986–35999. [[CrossRef](#)]
38. Wang, Y.; Liu, X.; Liu, J.; Han, B.; Hu, X.; Yang, F.; Xu, Z.; Li, Y.; Jia, S.; Li, Z.; et al. Carbon Quantum Dot Implanted Graphite Carbon Nitride Nanotubes: Excellent Charge Separation and Enhanced Photocatalytic Hydrogen Evolution. *Angew. Chem. Int. Ed.* **2018**, *57*, 5765–5771. [[CrossRef](#)] [[PubMed](#)]
39. Han, J.; Han, Z.; Da, X.; Yang, Z.; Zhang, D.; Hong, R.; Tao, C.; Lin, H.; Huang, Y. Preparation and photocatalytic activity of red light-emitting carbon dots/P25 heterojunction photocatalyst with ultra-wide absorption spectrum. *Mater. Res. Express* **2021**, *8*, 025002. [[CrossRef](#)]
40. Liu, W.; Li, Y.; Liu, F.; Jiang, W.; Zhang, D.; Liang, J. Visible-light-driven photocatalytic degradation of diclofenac by carbon quantum dots modified porous g-C<sub>3</sub>N<sub>4</sub>: Mechanisms, degradation pathway and DFT calculation. *Water Res.* **2019**, *151*, 8–19. [[CrossRef](#)]
41. Li, Y.Y.; Si, Y.; Zhou, B.X.; Huang, T.; Huang, W.Q.; Hu, W.; Pan, A.; Fan, X.; Huang, G.F. Interfacial charge modulation: Carbon quantum dot implanted carbon nitride double-deck nanoframes for robust visible-light photocatalytic tetracycline degradation. *Nanoscale* **2020**, *12*, 3135–3145. [[CrossRef](#)]
42. Wang, Y.; Zhang, M.; Zhao, J.; Chen, C.; Zhou, Y.; Zheng, X.; Zhang, C. In-situ one-step synthesis of porous monolayer carbon nitride nanosheets doped with carbon quantum dots for photocatalytic degradation of Meloxicam. *Colloids Surf. A Physicochem. Eng. Asp.* **2022**, *647*, 129042. [[CrossRef](#)]
43. Alkhouzaam, A.; Qiblawey, H.; Khraisheh, M. Polydopamine Functionalized Graphene Oxide as Membrane Nanofiller: Spectral and Structural Studies. *Membranes* **2021**, *11*, 86. [[CrossRef](#)] [[PubMed](#)]
44. Sun, D.; Mao, J.; Cheng, L.; Yang, X.; Li, H.; Zhang, L.; Zhang, W.; Zhang, Q.; Li, P. Magnetic g-C<sub>3</sub>N<sub>4</sub>/NiFe<sub>2</sub>O<sub>4</sub> composite with enhanced activity on photocatalytic disinfection of *Aspergillus flavus*. *Chem. Eng. J.* **2021**, *418*, 129417. [[CrossRef](#)]
45. Qiang, R.; Yang, S.; Hou, K.; Wang, J. Synthesis of carbon quantum dots with green luminescence from potato starch. *New J. Chem.* **2019**, *43*, 10826–10833. [[CrossRef](#)]
46. Zhang, L.; Zhang, J.; Xia, Y.; Xun, M.; Chen, H.; Liu, X.; Yin, X. Metal-Free Carbon Quantum Dots Implant Graphitic Carbon Nitride: Enhanced Photocatalytic Dye Wastewater Purification with Simultaneous Hydrogen Production. *Int. J. Mol. Sci.* **2020**, *21*, 1052. [[CrossRef](#)]
47. Li, K.; Su, F.-Y.; Zhang, W.-D. Modification of g-C<sub>3</sub>N<sub>4</sub> nanosheets by carbon quantum dots for highly efficient photocatalytic generation of hydrogen. *Appl. Surf. Sci.* **2016**, *375*, 110–117. [[CrossRef](#)]
48. Li, D.; Chen, W.; Sun, B.; Li, H.; Wu, T.; Ke, Q.; Huang, C.; Ei-Hamshary, H.; Al-Deyab, S.S.; Mo, X. A comparison of nanoscale and multiscale PCL/gelatin scaffolds prepared by disc-electrospinning. *Colloids Surf. B Biointerfaces* **2016**, *146*, 632–641. [[CrossRef](#)]

49. Scaffaro, R.; Lopresti, F.; Botta, L. Preparation, characterization and hydrolytic degradation of PLA/PCL co-mingled nanofibrous mats prepared via dual-jet electrospinning. *Eur. Polym. J.* **2017**, *96*, 266–277. [\[CrossRef\]](#)
50. Xu, Y.; Lin, W.; Wang, H.; Guo, J.; Yuan, D.; Bao, J.; Sun, S.; Zhao, W.; Zhao, C. Dual-functional polyethersulfone composite nanofibrous membranes with synergistic adsorption and photocatalytic degradation for organic dyes. *Compos. Sci. Technol.* **2020**, *199*, 108353. [\[CrossRef\]](#)
51. Mao, J.; Li, P.; Wang, J.; Wang, H.; Zhang, Q.; Zhang, L.; Li, H.; Zhang, W.; Peng, T. Insights into photocatalytic inactivation mechanism of the hypertoxic site in aflatoxin B<sub>1</sub> over clew-like WO<sub>3</sub> decorated with CdS nanoparticles. *Appl. Catal. B Environ.* **2019**, *248*, 477–486. [\[CrossRef\]](#)
52. Li, Q.H.; Dong, M.; Li, R.; Cui, Y.Q.; Xie, G.X.; Wang, X.X.; Long, Y.Z. Enhancement of Cr(VI) removal efficiency via adsorption/photocatalysis synergy using electrospun chitosan/g-C<sub>3</sub>N<sub>4</sub>/TiO<sub>2</sub> nanofibers. *Carbohydr. Polym.* **2021**, *253*, 117200. [\[CrossRef\]](#) [\[PubMed\]](#)
53. Shi, X.; Zhang, X.; Ma, L.; Xiang, C.; Li, L. TiO<sub>2</sub>-Doped Chitosan Microspheres Supported on Cellulose Acetate Fibers for Adsorption and Photocatalytic Degradation of Methyl Orange. *Polymers* **2019**, *11*, 1293. [\[CrossRef\]](#)
54. Li, S.; Luo, J.; Fan, J.; Chen, X.; Wan, Y. Aflatoxin B<sub>1</sub> removal by multifunctional membrane based on polydopamine intermediate layer. *Sep. Purif. Technol.* **2018**, *199*, 311–319. [\[CrossRef\]](#)
55. Yao, L.; Sun, C.; Lin, H.; Li, G.; Lian, Z.; Song, R.; Zhuang, S.; Zhang, D. Electrospun Bi-decorated Bi<sub>x</sub>Ti<sub>y</sub>O<sub>z</sub>/TiO<sub>2</sub> flexible carbon nanofibers and their applications on degrading of organic pollutants under solar radiation. *J. Mater. Sci. Technol.* **2022**, *150*, 114–123. [\[CrossRef\]](#)
56. Samsudin, M.F.R.; Frebillot, C.; Kaddoury, Y.; Sufian, S.; Ong, W.J. Bifunctional Z-Scheme Ag/AgVO<sub>3</sub>/g-C<sub>3</sub>N<sub>4</sub> photocatalysts for expired ciprofloxacin degradation and hydrogen production from natural rainwater without using scavengers. *J. Environ. Manag.* **2020**, *270*, 110803. [\[CrossRef\]](#) [\[PubMed\]](#)

**Disclaimer/Publisher's Note:** The statements, opinions and data contained in all publications are solely those of the individual author(s) and contributor(s) and not of MDPI and/or the editor(s). MDPI and/or the editor(s) disclaim responsibility for any injury to people or property resulting from any ideas, methods, instructions or products referred to in the content.